BMC Microbiology

RESEARCH Open Access

MotY modulates proton-driven flagellar motor output in *Pseudomonas aeruginosa*

Sanyuan Fu[1†], Maojin Tian[3†], Min Chen[1], Zhengyu Wu[2*], Rongjing Zhang[1*] and Junhua Yuan[1*]

Abstract

MotY homologs are present in a variety of monotrichous bacterial strains and are thought to form an additional structural T ring in flagellar motors. While MotY potentially plays an important role in motor torque generation, its impact on motor output dynamics remains poorly understood. In this study, we investigate the role of MotY in *P. aeruginosa*, elucidating its interactions with the two sets of stator units (MotAB and MotCD) using Förster resonance energy transfer (FRET) assays. Employing a newly developed bead assay, we characterize the dynamic behavior of flagellar motors in *motY* mutants, identifying MotY as the key functional protein to affect the clockwise bias of naturally unbiased motors in *P. aeruginosa*. Our findings reveal that MotY enhances stator assembly efficiency without affecting the overall assembly of the flagellar structure. Additionally, we demonstrate that MotY is essential for maintaining motor torque and regulating switching rates. Our study highlights the physiological significance of MotY in fine-tuning flagellar motor function in complex environments.

Keywords Stator, FRET, Bead assay, Flagellum, Bacterial motility

Introduction

Flagella widely exist in bacterial systems as locomotor organs. A flagellum consists of a basal body, a helical filament, and a flexible hook [1]. The core component, the flagellar rotary motor in the basal body, is embedded in the cell membrane and comprises two main parts: the rotor and the stator. The rotor controls motor directional switching under the mediation of the chemotaxis signal transduction network [2], while the stator forms multiple ion conduction channels, converting the energy of ion flux into mechanical power for torque generation [3]. Different types of stator component proteins conduct different driver ions. Common types include proton-type stator proteins MotAB/MotCD and sodium-type stator proteins PomAB/MotPS [4–7]. Stator-associated proteins MotX and MotY have been discovered in *Vibrio parahaemolyticus*, *Pseudomonas aeruginosa*, *Shewanella oneidensis*, and other bacterial strains [4, 8, 9]. While these proteins are not thought to be involved in the assembly of ion transport channels, their specific functions remain to be fully elucidated.

The crystal structure of MotY shows two distinct domains: a N-terminal domain ($MotY_N$), and a C-terminal domain ($MotY_C$). $MotY_N$ interacts with MotX and is essential for cell motility, while $MotY_C$ contains a peptidoglycan binding motif [10]. With the development of

†Sanyuan Fu and Maojin Tian contributed equally to this work.

*Correspondence:
Zhengyu Wu
wuzhy@mail.ustc.edu.cn
Rongjing Zhang
rjzhang@ustc.edu.cn
Junhua Yuan
jhyuan@ustc.edu.cn
[1]Hefei National Research Center for Physical Sciences at the Microscale and Department of Physics, University of Science and Technology of China, Hefei, Anhui 230026, China
[2]Research Center of Translational Medicine, Central Hospital Affiliated to Shandong First Medical University, Jinan, Shandong 250013, China
[3]Center of Translational Medicine, Zibo Central Hospital Affiliated to Binzhou Medical University, Zibo, Shandong 255036, China

cryo-electron microscopy and other technologies, it was found that MotY can generate a ring-like structure, the T ring, while MotX is located at the edge of the T ring [11]. In *Vibrio* species, the T ring is thought to promote the recruitment of stator units and enhance torque generation. MotX binds to the periplasmic region of PomB, while MotY interacts with the basal body [10]. Structural analysis previously revealed that the density corresponding to the T ring exhibits 13-fold symmetry, which aligns with the number of stator units, suggesting that it plays a potential role in motor power output [12, 13]. Knockout of *motY* leads to a complete loss of motility in some bacterial species. However, in *P. aeruginosa*, this mutation does not result in complete paralysis of the motor. Instead, it significantly alters the motility phenotype, such as impairing swimming motility [4]. In general, current research on MotY mainly focuses on structural biology and motor phenotype descriptions. However, the impact of MotY on output dynamics at the single motor level has not yet been accurately measured.

The opportunistic pathogen *P. aeruginosa* possesses two sets of stator units, MotAB and MotCD, both of which use proton motive force to power flagellar rotation and cooperate to enable cell movement in a variety of external environments [14]. *P. aeruginosa* uses a four-tiered transcriptional regulatory network to achieve precise control of flagellar biosynthesis [15]. The multiple ring structures contained in the basal body play crucial roles in structural stability and operational functionality [16]. Unlike *Vibrio* species that can only form a small T-ring in the absence of MotX [10], *P. aeruginosa* does not have a gene encoding MotX in its genome, and its complete T-ring assembly relies solely on MotY [17]. This characteristic creates favorable conditions for studying the impact of the non-conserved flagellar motor-related protein MotY on motor output. It allows retention of MotY's structural characteristics while avoiding the influence of its partner protein MotX.

Previously, the lack of stable motor output monitoring methods in strains that can endogenously produce MotY protein hindered detailed studies of MotY's dynamic characteristics. We recently developed a microbead labeling assay for *P. aeruginosa* flagellar filament stubs [18], which enables direct, long-term observation of motor output kinetics, addressing this experimental challenge.

In this study, we used the Förster resonance energy transfer (FRET) assay to elucidate the interaction between MotY and the stator units, which provides a structural basis for its influence on motor output. We further employed the bead assay to explore the function of MotY and found that the Δ*motY* mutant differed from the wild-type strain in multiple characteristics, including torque generation and switching rate. Notably, the Δ*motY* strain no longer maintains the unbiased motor characteristics of *P. aeruginosa*, thus revealing a key functional protein that affects the switching preference of this type of motor. Additionally, we used flagellar filament labeling technology to determine the proportion of individuals with flagellar filaments in the Δ*motY* strain and found that it did not differ from the wild-type. Gene editing techniques helped us discover that the unipolar assembly efficiency of stator proteins was reduced in the above mutants. Therefore, while MotY protein and its corresponding structure are important for the assembly of the stators, they do not affect the overall assembly efficiency of the flagellum.

Results

MotY interacts with both stator proteins MotB and MotD

In *Vibrio* species, the T ring is thought to achieve stator recruitment through the interaction between MotX and PomB. In contrast, the T ring of *P. aeruginosa* is composed solely of the MotY protein, and *P. aeruginosa* has two sets of stator units. To investigate the potential interactions between MotY and the stator units, we employed FRET, an assay using the energy transfer between two light-sensitive molecules where intermolecular distance is a key factor.

In a FRET assay, the interaction of a pair of donor and acceptor fluorescence proteins was examined. If an interaction exists, bleaching of the acceptor eliminates the energy transfer, causing an increase in donor fluorescence emission. We constructed an eCFP-MotY fusion as the donor, and eYFP-MotB and eYFP-MotD fusions as acceptors. FRET assays were performed for the eCFP-MotY/eYFP-MotB pair in the Δ*fliC*Δ*motAB*Δ*motY* strain, and for the eCFP-MotY/eYFP-MotD pair in the Δ*fliC*Δ*motCD*Δ*motY* strain. In both measurements, we found that CFP emission increased upon bleaching of YFP (Fig. 1), indicating energy transfer and protein interaction.

The FRET efficiency (E) was 1.72±0.96% for the eCFP-MotY/eYFP-MotB pair (N=16), and 1.54±0.55% for the eCFP-MotY/eYFP-MotD pair (N=12). Given that $E \geq 1\%$ is typically regarded as the threshold for strong FRET [19], our results suggest that MotY interacts strongly with both MotB and MotD. As a control, *ecfp-motY*-pME6032 was transformed into Δ*fliC*Δ*motAB*Δ*motY* and Δ*fliC*Δ*motCD*Δ*motY* strains, and no enhancement in the CFP channel was observed after bleaching (Fig. S1). To confirm whether the FRET occurred at the motor, we constructed strain Δ*fliC*Δ*motAB*Δ*motY* Δ*fliG* and conducted FRET assays by acceptor bleaching with eCFP-MotY/eYFP-MotB pairs (Fig. S2). FliG is the main component protein of the flagellar motor C ring [1], and the Δ*fliG* strain disrupted the assembly of the flagellar motor. We observed a notably reduced FRET signal (efficiency=1.38±0.33%, N=10) compared to the Δ*fliC*Δ*motAB*Δ*motY* strain. This suggests that while some interactions occur outside the fully assembled

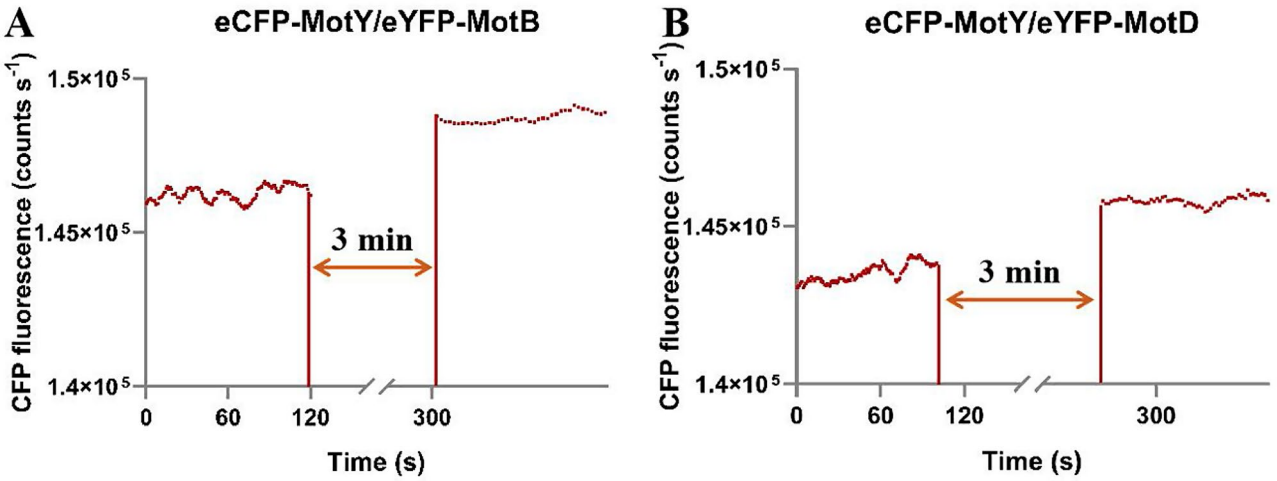

Fig. 1 FRET assays by acceptor bleaching with eCFP-MotY/eYFP-MotB and eCFP-MotY/eYFP-MotD pairs. (**A**) Representative FRET assay result for the eCFP-MotY/eYFP-MotB pair expressed in the Δ*fliC*Δ*motAB*Δ*motY* strain. Positive FRET is observed as an increase in CFP emission after YFP bleaching for 3 min. FRET efficiency $E = 1.72 \pm 0.96\%$ ($N = 16$) indicates a strong interaction between MotY and MotB. (**B**) Representative FRET assay result for the eCFP-MotY/eYFP-MotD pair in the Δ*fliC*Δ*motCD*Δ*motY* strain. $E = 1.54 \pm 0.55\%$ ($N = 12$) suggests a strong interaction between MotY and MotD

motor, a significant portion of the FRET signal is specific to motor-associated interactions.

We also test whether MotY, MotB, and MotD maintain their native function after fusion with fluorescent proteins. We conducted additional swimming plate assays on related strains (shown in Fig. S3). The introduction of exogenous eCFP-MotY and eYFP-MotD restored the motility of Δ*motY* and Δ*motD* strains, respectively, demonstrating that these fusion proteins retained their native functions. The strain expressing eYFP-MotB showed a reduced motility phenotype compared to the Δ*motB* strain. This suggests the existence of stator competition for occupancy. Specifically, eYFP-MotB likely occupied the original site of MotD due to its high expression level. As MotB does not support swimming in agar as well as MotD, this resulted in reduced motility. This observation is consistent with Baker et al. [20], who found that overexpression of MotAB protein in the wild-type strain caused a loss of swarming motility, further supporting the concept of dual stator competition for occupancy. In summary, the three fluorescent fusion proteins can reach the corresponding positions and function in the motor. Furthermore, we performed fluorescence imaging of the intracellular localizations of eCFP-MotY, eYFP-MotB, and eYFP-MotD (shown in Fig. S4). eYFP-MotB or eYFP-MotD bright spots were observed in some cells, although eCFP-MotY showed a more diffuse pattern.

Absence of MotY results in lower motor speed and higher motor switching rate

Structural analysis suggests that the T ring formed by MotY enhances motor torque generation, but direct evidence has been lacking. To address this, we attached micron-sized beads to the flagellar filament stubs of the *motY* knockout strain and used a high-speed camera to accurately record their trajectory, depicting single-motor level dynamic output.

We explored the effect of *motY* loss on the speed output of the motor. We measured the average rotation speeds for the Δ*motY* strain at 35.13 ± 10.56 Hz (counterclockwise, CCW) and 31.97 ± 10.32 Hz (clockwise, CW), nearly 30% lower than the wild-type (Fig. 2A), which rotated at 51.75 ± 9.06 Hz (CCW) and 48.51 ± 8.95 Hz (CCW) according to our previous study [18]. Motor torque decreased proportionally.

The switching rate of the wild-type strain was 0.42 ± 0.13 s^{-1}, while for the Δ*motY* mutant, it was 0.67 ± 0.43 s^{-1} (Fig. 2B), approximately 60% higher and with a significantly more dispersed data distribution. One-way analysis of variance (ANOVA) and paired-sample *t*-tests showed significant statistical differences in both motor speed and switching rate between the two strains (P-value<10^{-4}). Typical time traces of the wild-type and Δ*motY* strains are shown in Fig. 2C.

Additionally, we used the swimming plate assay to observe the macroscopic expansion behavior of the wild-type and several mutants (Fig. 2D, Fig. S5). This revealed that deletion of *motY* affects the environmental exploration ability of the bacterial population, and the combined knockout of *motY* and individual stator units further inhibits expansion. In particular, the Δ*motAB*Δ*motY* strain exhibits a phenotype similar to that of the Δ*motB*Δ*motCD* strain, suggesting a near-loss of motility.

Here, we clarified the role of MotY in the output of the flagellar motor of *P. aeruginosa* through the bead assay. As a non-conserved protein, MotY does not exist in strains with biased motors such as *Escherichia coli*, and there is no similar T-ring structure in the corresponding

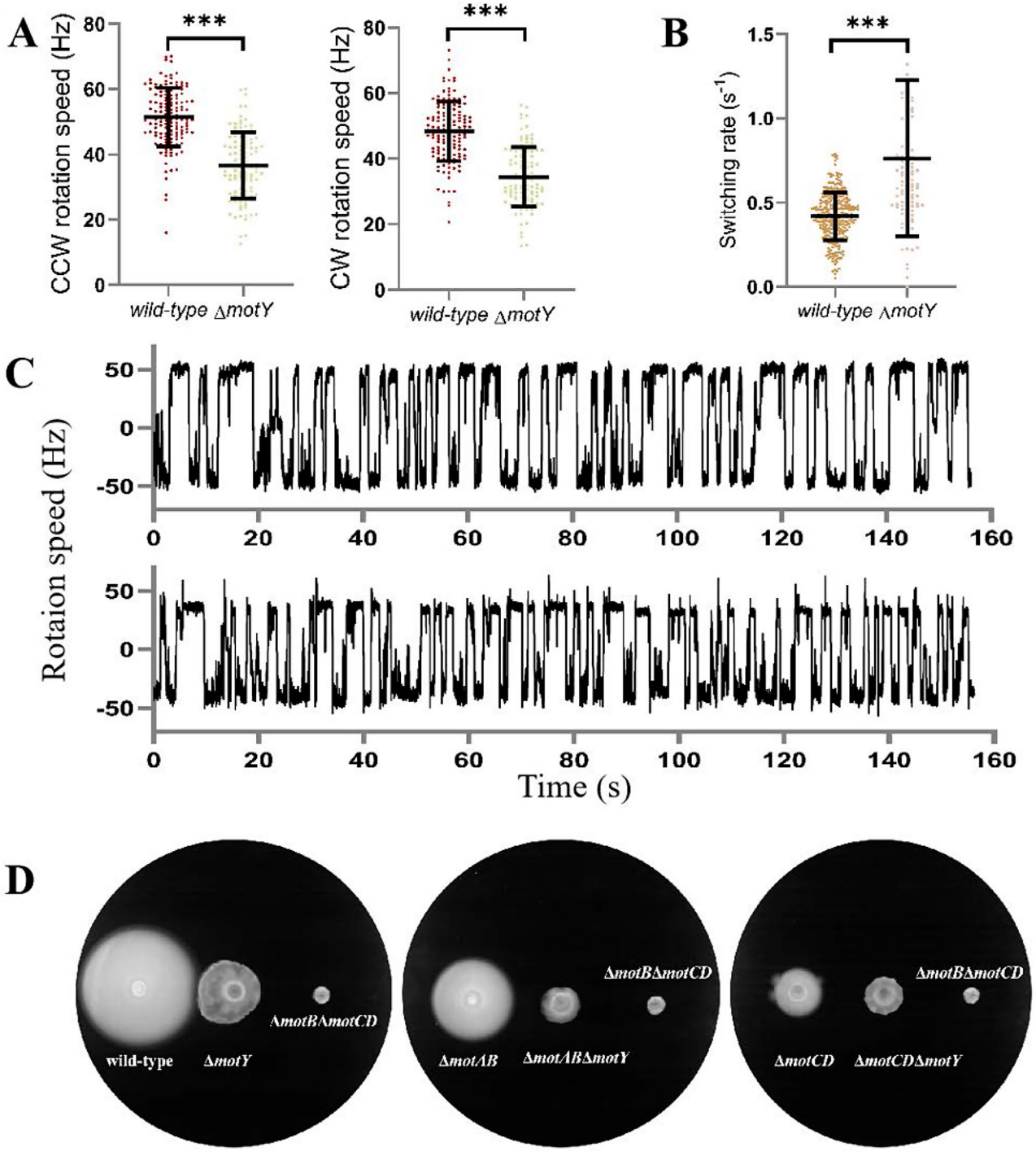

Fig. 2 MotY knockout affects multi-level motility-related phenotypes of *P. aeruginosa*. (**A**) Motor CCW and CW speeds for wild-type and Δ*motY* strains. The speed of the Δ*motY* strain ($N = 142$) is 30% lower than that of the wild-type strain. (**B**) Motor switching rate for wild-type and Δ*motY* strains. The switching rate of the Δ*motY* strain is 60% higher than that of the wild-type strain. '***': significant difference (P-value<0.0001). (**C**) Typical time traces of motor rotation speed for the wild-type (top) and Δ*motY* mutant (bottom). (**D**) Swimming-plate assays for the wild-type/Δ*motY*/Δ*motB*Δ*motCD*, Δ*motAB*/Δ*motAB*Δ*motY*/Δ*motB*Δ*motCD* and Δ*motCD*/Δ*motCD*Δ*motY*/Δ*motB*Δ*motCD* strains. Wild-type cells show a larger expansion radius than Δ*motY* mutants on swimming plates, suggesting that MotY deletion impairs the motility and environmental exploration ability of *P. aeruginosa*. Expansion of Δ*motAB*Δ*motY* and Δ*motCD*Δ*motY* was severely inhibited. All plates were photographed 16 h after inoculation

strains. Therefore, we aimed to further explore the effect of MotY on the switching preference of unbiased motor and extend the understanding of the physiological significance of the T ring.

T ring is the structural basis for ensuring the unbiased motor characteristics

For biased flagellar motors, CW bias is controlled by the core chemotaxis protein CheY-P. The number of CheY-P molecules binding to corresponding sites on the motor C ring directly affects the CW bias, thus elegantly connecting the motility and chemotaxis systems [21–23]. *P. aeruginosa* features an unbiased motor (with a CW bias of 0.5), and it is speculated that intracellular CheY-P concentration influences the switching rate of the motor without affecting its CW bias [24]. This unbiased nature is surprising, especially considering that factors such as specific intracellular protein concentrations vary among individual cells. This suggests that there may be structural elements that ensure the unbiased nature of the *P. aeruginosa* motor, which we sought to identify.

Previously, we found that the knockout of certain stator-related genes (Δ*motAB* and Δ*motCD*) primarily affects motor output in terms of torque generation and switching rate, while maintaining CW bias highly consistent with the wild-type strain [18]. Similar conclusions were later drawn for the knockout of the motor modulator *fliL* [25]. Notably, the stator units (MotAB and MotCD) dynamically associate with or dissociate from the rotor, while FliL is a connecting protein interacting with the stator and rotor. Neither generates permanent motor structures.

The T ring formed by MotY is a non-conserved ring structure in flagellar motors. We further explored whether MotY affects motor CW bias. Figure 3 shows the CW bias distribution of several strains, with the Δ*motY* mutant exhibiting an average value of 0.31 ± 0.17, significantly different from other strains. Additionally, exclusively CCW-rotating individuals appeared in the Δ*motY* strain. Loss of MotY disrupts the unbiased nature of the *P. aeruginosa* flagellar motor and amplifies phenotypic differences between individuals within a population. Transformation of the Δ*motY* mutant strain with a MotY expression plasmid restored the motor's unbiasedness (Fig. 3), further supporting this conclusion.

Stator assembly efficiency, but not overall flagellar assembly efficiency, is affected by MotY deletion

At the single motor level, the T ring increases torque generation and ensures CW bias characteristics. The known conserved motor ring structures are usually indispensable links in the flagellar assembly process. For example, flagella (including the motors) in MS ring or C ring mutants are unable to assemble completely [26–28]. We sought to investigate whether the absence of the T ring would affect the assembly of flagella to clarify its structural significance.

Previously, by introducing amino acid mutations into the flagellar filament protein FliC, in vivo visualization of flagellar filaments was achieved [29]. As the extension of flagellar filaments is the last step in flagellar assembly, flagellar assembly efficiency can be measured by quantitatively analyzing the growth of flagellar filaments. We performed flagellar fluorescence imaging for the

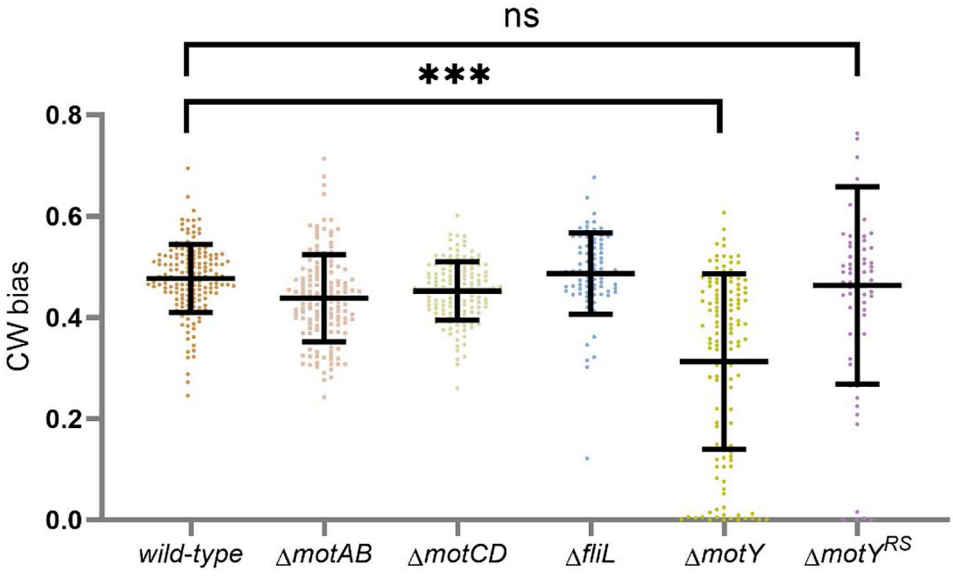

Fig. 3 CW bias distribution of several *P. aeruginosa* strains. *P. aeruginosa* has an unbiased motor. The loss of stable structural proteins (FliL) or dynamic assembly proteins (MotAB or MotCD) does not alter this unbiased nature, while the loss of MotY disrupts this fundamental property. '***': significant difference (P-value<0.0001), 'ns.': no significant difference (P-value>0.05). Δ*motY*^{RS} indicates the Δ*motY* strain transformed with a plasmid expressing MotY

wild-type and Δ*motY* strains (Fig. 4A). Statistical analysis showed that 84.40% (N=1494) of Δ*motY* cells had clear flagellar filaments (Fig. S6A), similar to the wild-type strain (82.15%, N=2095), suggesting that the loss of the T ring does not affect overall flagellar assembly efficiency.

We then explored whether the loss of MotY would affect the assembly of the stator units. Gene editing technology was used to fuse EGFP to the N-terminus of MotD. There is a strong asymmetry in the expression levels of MotAB and MotCD stator proteins, with MotAB expressing several times more than MotCD [30]. In light of this, we fused mEGFP, which disperses well and is less prone to aggregation, with MotB. The construction of these fluorescent fusion proteins enabled more accurate information gathering. As the dynamic assembly of stator units occurs near the cell membrane, we used TIRF microscopy to avoid background fluorescence interference (Fig. 4B). Statistical analysis of over 3,000 cells showed that the probability of unipolar fluorescent bright spots of the stator units (MotB and MotD) decreased by about 30% after *motY* knockout (Fig. S6B), indicating that *motY* deletion affects stator assembly efficiency.

Summary and discussion

The stator system is an indispensable component in flagellar motors. Ion transport channels, assembled with stator proteins, provide the energy source necessary for the smooth operation of the motor. The flagellar stator unit is a 5:2 complex composed of five molecules of MotA or MotC and two molecules of MotB or MotD, and is relatively conserved across motile bacteria, independent of the type of driving ion [31]. MotY, a stator protein analog discovered over 20 years ago, has been localized at the micrometer level using fluorescence imaging. Recent advancements in cryo-electron microscopy have increased the resolution of its structure to the nanometer level. However, research on MotY's actual physiological function has been lacking, with motility studies primarily limited to phenotypic observations. This study aims to address this gap by employing multiple technical approaches.

In *P. aeruginosa*, MotY can independently generate the complete motor T-ring without relying on MotX. The recent development of flagellar microbead labeling technology for *P. aeruginosa* flagellar motor by our team has enabled the monitoring of single motor dynamics over extended periods. These characteristics make *P. aeruginosa* an ideal model for studying the physiological effects

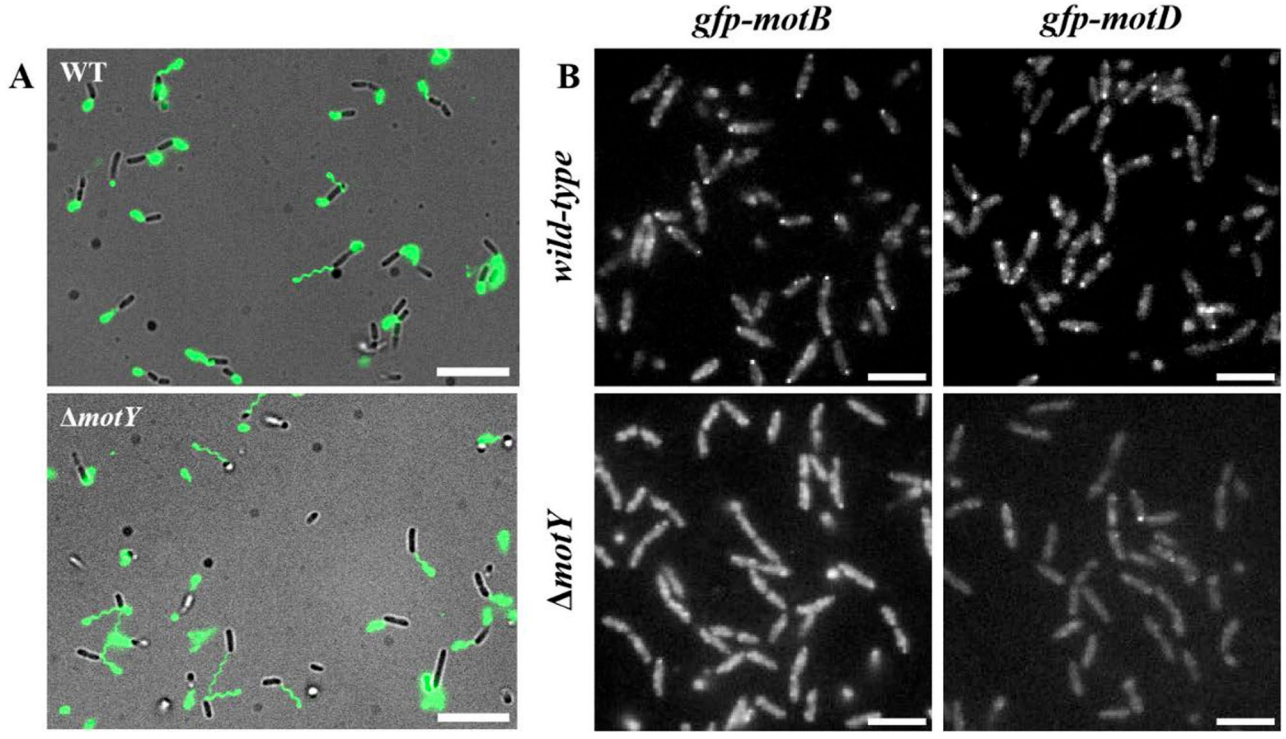

Fig. 4 Effect of *motY* deletion on flagellar and stator unit assembly efficiencies in *P. aeruginosa*. (**A**) The *motY* mutant exhibited flagellar assembly efficiency similar to that of the wild-type strain. Endogenous flagellar filament protein FliC for the wild-type (top) and Δ*motY* (bottom) strains was labeled with maleimide-AlexaFluor568 and visualized by phase contrast and fluorescence microscopy. Scale bar: 10 μm. (**B**) MotY deletion affects the dynamic assembly efficiency of the stator units. Cellular localization of EGFP-fused MotB and MotD in the wild-type and Δ*motY* strains was observed using a TIRF microscope. Scale bar: 5 μm

of MotY. We first demonstrated the interaction between MotY and the two stator proteins (MotB and MotD) using FRET experiments. Subsequently, we employed the bead assay to systematically study the effect of MotY on *P. aeruginosa* motors. The loss of MotY results in decreased motor speed, with quantitative analysis revealing a 40% reduction in torque generation compared to the wild-type strain, along with an increased switching rate. These changes are reflected not only in mean values but also in wider value distributions for the Δ*motY* mutant, suggesting that the loss of the T-ring has an impact on stator binding, thereby increasing inter-individual differences. Furthermore, through swimming plate and single-cell tracking assays, we found that *motAB* and *motY* double knockout strains almost completely lost their motility. The *motCD* and *motY* double knockout strains exhibited phenotypes similar to the Δ*motCD* strain in characteristics such as switching rate. This suggests that the MotAB stator is relatively independent, while the possibility of a closer interconnected structural relationship between MotCD and MotY warrants further discussion.

The unbiased nature of the *P. aeruginosa* flagellar motor is intriguing. Early single-cell chemotaxis experiments suggested that intracellular CheY-P concentration affects motor switching rate without altering CW bias. Unlike biased motors, additional structural features may be responsible for this unbiased nature. MotY, the sole component of the T ring, became the focus of our investigation. Through measurement and analysis of 142 Δ*motY* cells, we found that the average CW bias dropped to around 0.3, a decrease of nearly 40%. Notably, we identified exclusively CCW-rotating motors in the Δ*motY* strain. Motor rotation direction changes are typically associated with C ring conformational changes. Based on these observations, we hypothesize that the T ring, composed of MotY, serves a dual function: it interacts with the stator unit to enhance motor torque output and with the C ring to maintain switching stability. This provides a preliminary experimental basis for exploring the molecular mechanism underlying the unbiased operation of the *P. aeruginosa* flagellar motor. Further exploration into the dynamic effects of other flagellar proteins will help to fully elucidate this phenomenon.

Our studies have elucidated that MotY plays a crucial role in torque generation, similar to a stator unit, with the MotY-assembled T ring acting as a supporting element. Flagellar assembly follows a precise internal logic, involving dozens of proteins in an orderly manner. While the binding and unbinding of stator units occur dynamically without affecting flagellar assembly efficiency, the absence of conserved ring structures (MS ring or C ring) halts flagellar assembly at an early stage. The extension of flagellar filaments into extracellular space marks the final step of flagella assembly. Thus, the proportion of individuals with flagellar filaments serves as an indicator of flagellar assembly efficiency. Statistical analysis revealed that the Δ*motY* mutant exhibited flagellar assembly efficiency comparable to that of the wild-type. Given that the loss of MotY does not affect overall flagellar assembly efficiency, we investigated its impact on the dynamic assembly of the two sets of stator units. Using gene editing technology, we constructed strains expressing meGFP-MotB and eGFP-MotD. Our observations showed a decreased probability of MotB and MotD localization at the cell pole, suggesting that T ring assembly is a prerequisite for stator complex formation.

Materials and methods

Strains and cell culture

All strains and plasmids used in this study are listed in Table 1. The Δ*fliC*Δ*motY* strain was constructed to clarify the effect of MotY on the dynamic output of the flagellar motor. The mutant *fliC* allele, $fliC^{T394C}$, introduces free thiol groups into the flagellin protein to facilitate subsequent diversified modification. The plasmid $fliC^{T394C}$-pJN105 was transformed into the Δ*fliC* strain by electroporation for the bead assay and flagellar filament labeling. The *motY* gene was further knocked out in the existing Δ*fliC*Δ*motAB* and Δ*fliC*Δ*motCD* strains [18]. The plasmids *eyfp-motB*/*motD*-pJN105 and *ecfp-motY*-pME6032 were electroporated into the above strains in pairs for the FRET experiments. The vector *motY*-pME6032 was constructed for protein function restoration experiments. Fluorescent proteins fused to the N-terminus of stator proteins (MotB and MotD) were used to visualize their distribution. The *Escherichia coli* TOP10 strain was used for standard genetic manipulations.

A single-colony isolate was grown overnight in 3 ml LB broth (1% Bacto Tryptone, 0.5% Yeast Extract and 1% NaCl) on a rotary shaker (250 rpm) at 37 °C, and then diluted 1:100 into 10 ml of fresh LB broth to grow to the exponential phase. Appropriate antibiotics were added if necessary to prevent plasmid loss: for *E. coli*, 15 μg/ml Gentamicin and 12.5 μg/ml Tetracycline; for *P. aeruginosa*, 30 μg/ml Gentamicin and 50 μg/ml Tetracycline. To induce protein expression, 0.3 mM Isopropyl β-D-1-thiogalactopyranoside (IPTG) was added to strains with pME6032-derivative vectors, and 0.05% arabinose was added to strains with pJN105-derivative vectors. The cell culture was harvested by centrifugation (4000 × *g* for 2 min), washed twice in motility buffer (MB) consisting of 0.15 M NaCl, 50 mM potassium phosphate, 10 mM DL-lactic acid, 5 mM $MgCl_2 \cdot 7H_2O$ and 15 μM EDTA (pH = 7.0) [18, 24], and then resuspended in the same buffer.

Table 1 Strains and plasmids used in this study

Strain, Plasmid	Genotype, phenotype, and Description	Source
Strains		
P. aeruginosa		
PAO1	wild-type strain	Fan Jin Group
Δ*fliC*	nonpolar *fliC* deletion in PAO1	Fan Jin Group
Δ*fliC* Δ*motY*	nonpolar *motY* deletion in Δ*fliC*	This study
Δ*fliC* Δ*motAB*	nonpolar *motAB* deletion in Δ*fliC*	Ref 18
Δ*fliC* Δ*motCD*	nonpolar *motCD* deletion in Δ*fliC*	Ref 18
Δ*fliC* Δ*motAB* Δ*motY*	nonpolar *motY* deletion in Δ*fliC* Δ*motAB*	This study
Δ*fliC* Δ*motCD* Δ*motY*	nonpolar *motY* deletion in Δ*fliC* Δ*motCD*	This study
Δ*fliC* Δ*motAB* Δ*motY* Δ*fliG*	nonpolar *fliG* deletion in Δ*fliC* Δ*motAB*Δ*motY*	This study
Δ*motB*	nonpolar *motB* deletion in PAO1	This study
Δ*motD*	nonpolar *motD* deletion in PAO1	This study
Δ*motB* Δ*motCD*	nonpolar *motCD* deletion in Δ*motB*	This study
megfp-motB	*megfp* fusions at the N-terminus of *motB* in PAO1	This study
egfp-motD	*egfp* fusions at the N-terminus of *motD* in PAO1	This study
Δ*motY megfp-motB*	nonpolar *motY* deletion in *megfp-motB*	This study
Δ*motY egfp-motD*	nonpolar *motY* deletion in *egfp-motD*	This study
E. coli		
Top10	F-*mcrA* Δ(*mrr-hsRMS-mcrBC*)Φ80*lacZ* Δ*M15* Δ*lacX74 recA1* *ara* D139 Δ*(araleu)* 7697 *galU galK rpsL(*Nal^R*)* endA1 *nupG*	Invitrogen
Plasmids		
pex18gm	$oriT^+sacB^+$; gene replacement vector with MCS from pUC18; Gm^r	Fan Jin Group
motY -pex18gm	In-frame deletion of *motY* cloned into pex18gm; Gm^r	This study
megfp-motB -pex18gm	*megfp* fusions *motB* cloned into pex18gm; Gm^r	This study
egfp-motD -pex18gm	*egfp* fusions *motD* cloned into pex18gm; Gm^r	This study
fliG-pex18gm	In-frame deletion of *fliG* cloned into pex18gm; Gm^r	This study
motB -pex18gm	In-frame deletion of *motB* cloned into pex18gm; Gm^r	This study
motD -pex18gm	In-frame deletion of *motD* cloned into pex18gm; Gm^r	This study
eyfp -motB -pJN105	*eyfp-motB* overexpression vector in pJN105, P_{BAD} promoter; Gm^r	Ref 25
eyfp -motD -pJN105	*eyfp-motD* overexpression vector in pJN105, P_{BAD} promoter; Gm^r	Ref 25
ecfp-motY -pME6032	*ecfp-motY* overexpression vector in pME6032, P_{Lac} promoter; Tec^r	This study
$fliC^{T394C}$-pJN105	$fliC^{T394C}$ overexpression vector in pJN105, P_{BAD} promoter; Gm^r	Ref 18
motY -pME6032	*motY* overexpression vector in pME6032, P_{Lac} promoter; Tec^r	This study

Construction of gene deletion mutants in *P. aeruginosa*

A two-step allelic recombination method was used to construct knockout strains [32]. We used polymerase chain reaction (PCR) to generate ~1000-bp DNA fragments with upstream and downstream sequences flanking the gene targeted for deletion (residues 100 to 687 were deleted in the *motY* mutant). The linearized pex18gm vector was fused with the above two PCR fragments using Gibson assembly [33], and the resulting plasmid was electroporated into *P. aeruginosa*. For double screening, gentamicin plates (LB plates with 30 μg/ml gentamicin) and sucrose plates (NaCl-free LB plates with 15% sucrose) were used. Positive selection was finally confirmed by PCR and sequencing. In this study, three strains, Δ*fliC*Δ*motY*, Δ*fliC*Δ*motAB*Δ*motY*, and Δ*fliC*Δ*motCD*Δ*motY*, were constructed based on the existing strains of our group.

Generation of chromosomal fusions of fluorescent protein-encoding gene to *motB/motD*

We fused the gene encoding green fluorescent protein to the *motB/motD* gene at their native chromosomal loci to ensure expression similar to that in their wild-type counterparts. The construction of *megfp-motB/egfp-motD* is modeled on the method used for *gfp-motB* in *E. coli*. The putative membrane-targeting sequence of *motB* and *motD* was identified by sequence comparison with *motB* in *E. coli* (shown in Fig. S7A). A construct was generated that included 1000 bp upstream of *motB/motD*, incorporating the first 26 codons of *motB* (encompassing the putative membrane-targeting sequence), followed by *megfp* and then the complete sequence of *motB*. Similarly, the construct included the first 19 codons of *motD*, followed by *egfp* and then the complete sequence

of *motD*. This construct was assembled using Gibson assembly and inserted into chromosome by homologous recombination. The chromosome sequence after recombinant is shown in Fig. S7B.

FRET assay

CFP and YFP, a well-known FRET-generating protein pair, were used in this study to explore the interaction between MotY and MotB/MotD. The fluorescent fusion protein eCFP-MotY was expressed by the vector *ecfp-motY*-pME6032 under control of an IPTG-inducible promoter. The fusion proteins eYFP-MotB and eYFP-MotD were expressed from *eyfp-motB*-pJN105 and *eyfp-motD*-pJN105, respectively, under control of an L-arabinose-inducible promoter. The setup used here is similar to that described previously and is briefly summarized below [25, 34]. The cells were mounted on a poly-L-lysine coated coverslip, which was assembled to the sample chamber and placed on a Nikon Ti-E microscope with a 40× objective. The excitation light passed through a bandpass filter (438/24), and the emission light was divided into two channels (cyan and yellow) by a dichroic mirror. The light beams passed through the corresponding bandpass filters (483/32 for cyan and 542/32 for yellow) and were collected by independent photon-counting photomultipliers. The signal acquisition frequency was set at 1 Hz, the eYFP protein bleaching time was 180 s, and the signal intensity of the CFP channel before and after bleaching was extracted. The FRET efficiency was determined as $E = (F_1 - F_0)/F_1$, where F_1 was the CFP emission after bleaching and F_0 was the CFP emission before bleaching.

Swimming-plate assay

The ability of natural exploration was qualitatively examined using soft-agar swimming plates. Polystyrene Petri plates (150 mm in diameter) were filled with 30 ml of swim agar (0.3% Bacto agar, 1% Bacto tryptone, 0.5% yeast extract, and 1% NaCl, supplemented with 0.05% arabinose and antibiotics as needed). The plates were inoculated with 4 µl of fresh cultures of the corresponding strains. The swimming plates were incubated at 37 °C for 16 h, and then the radii of the swimming zones were measured.

Single-cell tracking assay

The bacterial solution was injected into a chamber constructed by attaching a clean coverslip to a glass slide with two pieces of double-sticky tape. The chamber was sealed with grease, and each sealed chamber was used for at most 20 min to ensure a relatively constant external environment for the cells. Cell motile behavior was observed using a Nikon Ti-E phase-contrast microscope with a 20× objective and recorded with an sCMOS camera (Thorlabs, DCC3240) at 50 fps. At least six videos, each lasting several minutes, were collected for each strain.

To quantify the active proportion of swimming individuals, we calculated the instantaneous velocity of the bacteria to determine whether the bacteria in the area were active or not. For every 10 s, the adjacent 10 frames of images were analyzed to calculate the cell trajectories. Bacteria with a mean velocity above 10 µm/s and a mean squared displacement (MSD) slope above 1.2 from a log-log fit were classified as motile individuals. We then averaged the number of motile bacteria and total bacteria in each video. The data from all videos were averaged to determine the proportion of swimming individuals for each strain.

Bead assay

The bead assay used here was derived from our previous study [18]. The protocol followed is briefly described below. The filaments of bacteria were sheared by passing 1 ml of the washed-cell suspension 200 times between two syringes with 23-gauge needles, connected by 7-cm-long polyethylene tubing (inside diameter of 0.58 mm). The sheared 1 ml suspension was centrifuged at 4000 × *g* for 2 min, and the supernatant was discarded. 500 µl of MB was then added to resuspend the bacteria. We biotinylated the filaments by adding 5 µl of maleimide-PEG_2-biotin solution (Thermo Scientific, 10 mg/ml in DMSO) to the condensed cells and incubating for 20 min at room temperature with gyrorotation of 200 rpm, and then washing twice (4000 ×*g*, 2 min) and resuspending in 500 µl MB.

To measure the dynamic properties of the motor for Δ*motY* strain, each single motor was observed for 3 min. We constructed a sample chamber by attaching a poly-L-lysine coated coverslip to a glass slide with two pieces of double-sticky tape. 50 µl of treated cells was injected into the chamber and incubated for 5 min, and the unstuck cells were rinsed with 200 µl MB. A solution of 1-µm-diameter streptavidin-modified beads (Invitrogen-Molecular Probes) was washed in phosphate-buffered saline (PBS), resuspended in MB, and then added into the chamber to spontaneously attach to the biotinylated flagellar filaments. The chamber was sealed with grease and each sealed chamber was used for at most 20 min to ensure a relatively constant external environment for the cells. In this study, the bead-assay data for the wild-type came from our previous study [18]. We followed the same experimental conditions and data analysis methods in all experiments, which provided the basis for the consistency of the experimental results.

Flagellar staining and fluorescence imaging

Flagellar filaments were labeled by following the protocol described previously [35]. Cells (1 ml of

exponential-phase culture) were harvested by centrifugation at 1000 × *g* for 10 min and washed twice in 1 ml MB. The final pellet was adjusted to a volume of ~ 500 µl. Alexa Fluor 568 maleimide (Invitrogen-Molecular Probes) was used to label filaments (23℃, 30 min, conc. 20 µg/ml), and unused dye was washed away with MB. Cells containing fluorescent proteins were centrifuged and resuspended in MB, which were then placed at 37 °C for 30 min to allow protein maturation.

For fluorescence imaging, 50 µl of pre-treated bacterial solution was introduced into the chamber, which contained a coverslip coated with poly-L-lysine to fix the cells. After incubation for 3 min, 200 ml MB was used to wash away the excess cells. The boundary of the chamber was then sealed with Apiezon vacuum grease. A Nikon Ti-E microscope equipped with a 100× oil-immersion objective and a sCMOS camera (Prime95B, Photometrics) was used to observe the samples. To determine the proportion of individuals with flagella, bright field and fluorescence images were collected separately, using a 100 ms exposure time. The fluorescent images of meGFP -MotB and eGFP-MotD were taken with a 200 ms exposure, and the experiment was performed on a Nikon Ti-E TIRF microscope equipped with an EMCCD camera (Andor iXon 897) and a 100×1.49-NA oil-immersion TIRF objective.

Data analysis

Data analysis was performed using custom scripts in MATLAB. We converted the x and y positions of the bead into polar coordinates to calculate the angular velocity (CW positive and CCW negative) as described previously [36]. The two most probable velocities were considered to be the steady-state CCW and CW rotation velocities. Three velocity intervals were divided between the two steady-state velocities, and transitions between the top and bottom intervals were considered to be the switching events of the motor. Torque was calculated as the product of the rotational friction drag coefficient and the angular velocity, following the formula $8\pi\ \gamma\ {r_b}^3 + 6\pi\ \gamma\ r_b {r_r}^2$, where γ was the viscosity of the medium, r_b was the radius of the bead, and r_r was the rotational eccentricity [37].

Supplementary Information

The online version contains supplementary material available at https://doi.org/10.1186/s12866-024-03602-z.

Supplementary Material 1

Acknowledgements
Not applicable.

Author contributions
J.Y., R.Z. and Z.W. designed the work; S.F., Z.W. and M.T. performed the measurements with the help of M.C.; J.Y., R.Z. and Z.W. wrote the paper. S.F. and M.T. contributed equally to this work.

Funding
This work was supported by National Natural Science Foundation of China Grants (11925406, 12090053, 12304241, and 12304251), a grant from the Ministry of Science and Technology of China (2019YFA0709303), and Grants from the Natural Science Foundation of Shandong Province No. ZR2023QA111 and ZR2023QC168.

Data availability
All data generated or analyzed during this study are included. The data set used and /or analyzed during the current study is available from the corresponding author on reasonable request.

Declarations

Ethics approval and consent to participate
Not applicable.

Consent for publication
Not applicable.

Competing interests
The authors declare no competing interests.

Received: 27 August 2024 / Accepted: 23 October 2024
Published online: 08 November 2024

References

1. Wadhwa N, Berg HC. Bacterial motility: machinery and mechanisms. Nat Rev Microbiol. 2022;20:161–73.
2. Blair DF. Fine structure of a fine machine. J Bacteriol. 2006;188:7033–5.
3. Hu H, Santiveri M, Wadhwa N, Berg HC, Erhardt M, Taylor NMI. Structural basis of torque generation in the bi-directional bacterial flagellar motor. Trends Biochem Sci. 2022;47:160–72.
4. Doyle TB, Hawkins AC, McCarter LL. The complex flagellar torque generator of *Pseudomonas aeruginosa*. J Bacteriol. 2004;186:6341–50.
5. Kojima S, Blair DF. Solubilization and purification of the MotA/MotB complex of *Escherichia coli*. Biochemistry. 2004;43:26–34.
6. Yonekura K, Maki-Yonekura S, Homma M. Structure of the flagellar motor protein complex PomAB: implications for the torque-generating conformation. J Bacteriol. 2011;193:3863–70.
7. Ito M, Terahara N, Fujinami S, Krulwich TA. Properties of motility in *Bacillus subtilis* powered by the H+-coupled MotAB flagellar stator, Na+-coupled MotPS or hybrid stators MotAS or MotPB. J Mol Biol. 2005;352:396–408.
8. Koerdt A, Paulick A, Mock M, Jost K, Thormann KM. MotX and MotY are required for flagellar rotation in *Shewanella oneidensis* MR-1. J Bacteriol. 2009;191:5085–93.
9. Okunishi I, Kawagishi I, Homma M. Cloning and characterization of *motY*, a gene coding for a component of the sodium-driven flagellar motor in *Vibrio alginolyticus*. J Bacteriol. 1996;178:2409–15.
10. Kojima S, Shinohara A, Terashima H, Yakushi T, Sakuma M, Homma M, et al. Insights into the stator assembly of the *Vibrio* flagellar motor from the crystal structure of MotY. Proc Natl Acad Sci U S A. 2008;105:7696–701.
11. Terashima H, Fukuoka H, Yakushi T, Kojima S, Homma M. The *Vibrio* motor proteins, MotX and MotY, are associated with the basal body of Na-driven flagella and required for stator formation. Mol Microbiol. 2006;62:1170–80.
12. Beeby M, Ribardo DA, Brennan CA, Ruby EG, Jensen GJ, Hendrixson DR. Diverse high-torque bacterial flagellar motors assemble wider stator rings using a conserved protein scaffold. Proc Natl Acad Sci USA. 2016;113:E1917–26.
13. Zhu S, Nishikino T, Hu B, Kojima S, Homma M, Liu J. Molecular architecture of the sheathed polar flagellum in *Vibrio alginolyticus*. Proc Natl Acad Sci USA. 2017;114:10966–71.
14. Harshey RM. Bacterial motility on a surface: many ways to a common goal. Annu Rev Microbiol. 2003;57:249–73.

15. Dasgupta N, Wolfgang MC, Goodman AL, Arora SK, Jyot J, Lory S, et al. A four-tiered transcriptional regulatory circuit controls flagellar biogenesis in *Pseudomonas aeruginosa*. Mol Microbiol. 2003;50:809–24.
16. Kaplan M, Subramanian P, Ghosal D, Oikonomou CM, Pirbadian S, Starwalt-Lee R, et al. In situ imaging of the bacterial flagellar motor disassembly and assembly processes. EMBO J. 2019;38:e100957.
17. Zhu S, Schniederberend M, Zhitnitsky D, Jain R, Galan JE, Kazmierczak BI, et al. In Situ Structures of Polar and Lateral Flagella Revealed by Cryo-Electron Tomography. J Bacteriol. 2019;201:e00117–19.
18. Wu Z, Tian M, Zhang R, Yuan J. Dynamics of the Two Stator Systems in the Flagellar Motor of *Pseudomonas aeruginosa* Studied by a Bead Assay. Appl Environ Microbiol. 2021;87:e01674–21.
19. Li H, Sourjik V. Assembly and stability of flagellar motor in *Escherichia coli*. Mol Microbiol. 2011;80:886–99.
20. Baker AE, Webster SS, Diepold A, Kuchma SL, Bordeleau E, Armitage JP, et al. Flagellar Stators Stimulate c-di-GMP Production by *Pseudomonas aeruginosa*. J Bacteriol. 2019;201:00741–18.
21. Cluzel P, Surette M, Leibler S. An ultrasensitive bacterial motor revealed by monitoring signaling proteins in single cells. Science. 2000;287:1652–5.
22. Sourjik V, Berg HC. Binding of the *Escherichia coli* response regulator CheY to its target measured in vivo by fluorescence resonance energy transfer. Proc Natl Acad Sci USA. 2002;99:12669–74.
23. Welch M, Oosawa K, Aizawa S, Eisenbach M. Phosphorylation-dependent binding of a signal molecule to the flagellar switch of bacteria. Proc Natl Acad Sci USA. 1993;90:8787–91.
24. Cai Q, Li Z, Ouyang Q, Luo C, Gordon VD. Singly Flagellated *Pseudomonas aeruginosa* Chemotaxes Efficiently by Unbiased Motor Regulation. mBio. 2016;7:e00013–16.
25. Zhang L, Wu Z, Zhang R, Yuan J. FliL Differentially Interacts with Two Stator Systems To Regulate Flagellar Motor Output in *Pseudomonas aeruginosa*. Appl Environ Microbiol. 2022;88:e01539–22.
26. Kojima S, Nonoyama N, Takekawa N, Fukuoka H, Homma M. Mutations targeting the C-terminal domain of FliG can disrupt motor assembly in the Na(+)-driven flagella of *Vibrio alginolyticus*. J Mol Biol. 2011;414:62–74.
27. Levenson R, Zhou H, Dahlquist FW. Structural insights into the interaction between the bacterial flagellar motor proteins FliF and FliG. Biochemistry. 2012;51:5052–60.
28. Suzuki H, Yonekura K, Namba K. Structure of the rotor of the bacterial flagellar motor revealed by electron cryomicroscopy and single-particle image analysis. J Mol Biol. 2004;337:105–13.
29. Tian M, Wu Z, Zhang R, Yuan J. A new mode of swimming in singly flagellated *Pseudomonas aeruginosa*. Proc Natl Acad Sci USA. 2022;119:e2120508119.
30. de Anda J, Kuchma SL, Webster SS, Boromand A, Lewis KA, Lee CK, et al. How *P. aeruginosa* cells with diverse stator composition collectively swarm. mBio. 2024;15:e03322–23.
31. Santiveri M, Roa-Eguiara A, Kuhne C, Wadhwa N, Hu H, Berg HC, et al. Structure and Function of Stator Units of the Bacterial Flagellar Motor. Cell. 2020;183:244–57.
32. Hmelo LR, Borlee BR, Almblad H, Love ME, Randall TE, Tseng BS, et al. Precision-engineering the *Pseudomonas aeruginosa* genome with two-step allelic exchange. Nat Protoc. 2015;10:1820–41.
33. Gibson DG, Young L, Chuang RY, Venter JC, Hutchison CA, Smith HO. Enzymatic assembly of DNA molecules up to several hundred kilobases. Nat Methods. 2009;6:343–5.
34. Zhang C, He R, Zhang R, Yuan J. Motor Adaptive Remodeling Speeds Up Bacterial Chemotactic Adaptation. Biophys J. 2018;114:1225–31.
35. Turner L, Zhang R, Darnton NC, Berg HC. Visualization of Flagella during bacterial Swarming. J Bacteriol. 2010;192:3259–67.
36. Yuan J, Fahrner KA, Berg HC. Switching of the bacterial flagellar motor near zero load. J Mol Biol. 2009;390:394–400.
37. Inoue Y, Lo CJ, Fukuoka H, Takahashi H, Sowa Y, Pilizota T, et al. Torque-speed relationships of Na+-driven chimeric flagellar motors in *Escherichia coli*. J Mol Biol. 2008;376:1251–9.

Publisher's note